MULTISCALE MODEL. SIMUL.
Vol. 3, No. 1, pp. 131–150

A MULTISCALE DATA ASSIMILATION WITH THE ENSEMBLE KALMAN FILTER*

YU ZOU† AND ROGER GHANEM†

Abstract. In this paper, a multiscale data assimilation approach is constructed to evaluate boundary conditions for particle fluxes in numerical simulations of particle transport problems. An adaptation of the ensemble Kalman filtering (EnKF) method is used as the engine for estimation and filtering across scales. To implement this multiscale approach, a multiscale bridging model, which can predict the particle fluxes across arbitrary spatial intervals in any scale, is developed by considering particles undergoing transverse random walk emitted along a continuous boundary corresponding to the finest scale. In the model, particle fluxes across one scale are taken as the parameter set which is used to determine fluxes across another scale. The significance of this multiscale model is demonstrated through an example. Ensembles of Gaussian random processes of particle fluxes along the boundary are generated as the microscale model state according to a specified a priori information on the error covariance or spectral density functions. Measurements of particle quantities are taken at macroscale locations above the boundary and assimilated with model predictions to update the micro- and macroscale particle fluxes using the inverse analysis scheme of the multiscale EnKF approach. The updated random macroscale fluxes can be used as consistent boundary conditions for numerical simulations, such as large eddy simulation.

Key words. Kalman filter, multiscale data assimilation, probabilistic models

AMS subject classifications. 70G60, 37H10, 76R50, 76F65

DOI. 10.1137/030601168

1. Introduction.

Large eddy simulation (LES) has been the subject of significant research recently, in particular with regard to its applications in meteorology, hydrodynamics, and environmental turbulent flows [10, 12, 14]. An interesting feature of this class of methods is its suitability for linking with Lagrangian or Eulerian models of particle transport, allowing one to characterize not only the evolution of particle trajectories but also their dispersions and diffusivities [18, 13]. A challenge in linking LES to particle transport models relates to the proper specification of the particle flux along the boundary of the LES computational domain. A number of efforts for treating this problem have been proposed. Boundary conditions, such as elastic collisions and absorptions, have been introduced in LES simulations of particle-laden turbulent channel flows [18, 13], while boundary conditions on the particle concentration have been used, for instance, in the simulation of particle motions in the atmospheric boundary layer over a canopy of forest [5]. Neither of these conditions captures the random and dynamic character of the particle fluxes emitted from boundaries with arbitrary profiles. Ignoring the source mechanism of these particles and the randomness in their spatio-temporal evolution may significantly diminish the reliability of their predicted fate.

The correct representation of the dynamics of the boundary conditions is essentially an inverse problem which involves the assimilation of observables at the coarse scale to estimate sources at the finer scale. At the core of this inverse problem is a model for the dynamics in each of the interacting scales and a model for transitioning

*Received by the editors October 9, 2003; accepted for publication (in revised form) May 25, 2004; published electronically October 14, 2004. This work was supported by National Science Foundation grant 0119903.

http://www.siam.org/journals/mms/3-1/60116.html

†Department of Civil Engineering, The Johns Hopkins University, Baltimore, MD 21218 (zouyu@jhu.edu, Roger.Ghanem@jhu.edu).

information between them. This latter model, referred to as a bridging model, is typically a statement of some conservation law formulated in a multiscale context.

The probabilistic characterization of the fine-scale sources requires additional care in formulating the inverse problem. In particular, a probabilistic bridging model is now called upon to transfer probabilistic information across adjacent scales. In the present paper, a probabilistic mass conservation law is formulated and used that, while conserving mass globally, redistributes it locally according to some probabilistic law that is consistent with the prevailing physics.

Given the multiscale context of the class of problems of interest here, the geometry of the coarse scale appears, locally, as flat relative to the fine-scale dynamics. A canonical form of the problem can, therefore, be stated in terms of a fine-scale boundary of irregular geometry communicating, through a probabilistic bridging model, with a flat coarse-scale boundary. The ensemble Kalman filter approach is adopted, in conjunction with this bridging model, to assimilate information observed on the flat coarse-scale boundary into a probabilistic characterization of data at the fine scale.

The sequential data assimilation into models of dynamical systems originated from the standard Kalman filter (KF) [7, 8] for linear dynamic systems, which was subsequently generalized to treat nonlinear dynamical systems, in the form of the extended Kalman filter (EKF) [2, 6] and ensemble Kalman filter (EnKF) [1, 11, 17]. However, the EnKF gradually superseded the EKF due to its success in dealing with strongly nonlinear systems [3]. Moreover, the state error covariance matrix is never explicitly needed in the EnKF, as all error information is contained in the ensemble, which greatly reduces the computation load. Due to its advantages over other Kalman filtering methods, the EnKF is adopted in this paper to retrieve forecasts from the multiscale prediction for particle fluxes, and the updated particle fluxes in the macroscales are used to generate boundary conditions for numerical simulations.

This paper provides a bridging model to predict particle fluxes across an imaginary boundary for particles initially located on the finer-scale irregular boundary. This boundary represents a gateway to the coarse scale. The proposed bridging model, based on the assumption that particles move upward noninteractively with a Brownian motion in the transverse direction and the irregular boundary is absorbing, consists of first computing the probability of particles arriving at large-scale intervals from small-scale positions and then using the Monte Carlo simulation and the multinomial distribution to generate random particle fluxes in the large-scale flat boundary from those in the small-scale irregular boundary. The bridging model, along with the specified evolution model for fluxes in the original boundary, can be embedded in the multiscale data assimilation approach to provide estimation of true particle fluxes in the flat boundary and irregular boundary, respectively.

The specific dynamics associated with each of the fine and coarse scales are purposefully selected to be simple in order to highlight the associated methodology relevant to the EnKF assimilation procedure. Extensions to more complex evolution models at either scale can be readily developed and implemented once a meaningful bridging model has been identified. A procedure for that task, similar to the one developed here, could potentially be extended to more complex systems.

The next section of the paper presents the formulation of multiscale data assimilation using the EnKF. The multiscale bridging model for the prediction of boundary particle fluxes is presented in sections 3 and 4, respectively. Numerical results are shown in section 5 and conclusions presented in section 6.

2. General formulation for multiscale data assimilation using the EnKF. In engineering problems, different dynamical system models are usually used to describe phenomena in different scales. Two broad classes of problems typically present themselves in the context of multiscale data assimilation. In the first class, measurements are collected at a number of scales and used to update the state for each of these scales independently. In the second class of problems, measurements made at one scale can be made to bear on the predicted evolution of other scales. These two cases are treated separately in the next two subsections.

2.1. Data assimilation with uncoupled scales. The model state in each scale can be updated if the explicit system model and observation are available at that scale. Specifically, let the explicit discrete system models for different scales be given by

$$\boldsymbol{m}_{s,k+1} = \mathcal{L}_s(\boldsymbol{m}_{s,k}), \quad \boldsymbol{m} \in \mathbb{R}^n, \tag{2.1}$$

where $\boldsymbol{m}_{s,k}(\boldsymbol{x})$ represents the model state vector in scale s at time k, $\mathcal{L}_s(\cdot)$ is either a deterministic or a stochastic isomorphism on $\mathbb{R}^n$, and observation models are given by

$$\boldsymbol{z}_{s,k+1} = \mathcal{H}_s(\boldsymbol{m}_{s,k+1}) + \boldsymbol{v}_{s,k+1}, \quad \boldsymbol{z} \in \mathbb{R}^l, \quad \boldsymbol{v} \in \mathbb{R}^l, \tag{2.2}$$

where $\boldsymbol{z}_{s,k+1}$ is the observation in scale s at time $k+1$, $\mathcal{H}_s(\cdot) : \mathbb{R}^n \mapsto \mathbb{R}^l$ is either a linear or a nonlinear deterministic operator, and $\boldsymbol{v}_{s,k+1}$ is usually a temporally independent Gaussian random vector with zero mean. Then the ensemble Kalman filtering method can be applied to these models to obtain the updated model state. Accordingly, the conditional ensemble mean is taken as the Bayesian estimate of the model state, and the conditional covariance matrix around the mean is the error covariance for the estimate. Hence, based on the initial estimate for the state $\boldsymbol{m}_{s,0}$ and error covariance matrix, initial ensembles for the model states are generated, which are denoted by $\boldsymbol{m}^r_{s,0}$, $r = 1, \ldots, N_e$, where N_e is the ensemble size.

In the forecast step, a predicted value of $\boldsymbol{m}_{s,k+1}$ associated with the rth realization in the ensemble is obtained as

$$\boldsymbol{m}^r_{s,k+1|k} = \mathcal{L}_s(\boldsymbol{m}^r_{s,k}), \quad r = 1, \ldots, N_e, \tag{2.3}$$

with a corresponding predicted value for the observation given by

$$\boldsymbol{h}^r_{s,k+1|k} = \mathcal{H}_s(\boldsymbol{m}^r_{s,k+1|k}), \quad r = 1, \ldots, N_e. \tag{2.4}$$

The Kalman gain matrix can then be derived as [11]

$$\boldsymbol{K}_{s,k+1} = \boldsymbol{C}_{\boldsymbol{mh}}(\boldsymbol{C}_{\boldsymbol{hh}} + \boldsymbol{C}_{\boldsymbol{vv}})^{-1}, \tag{2.5}$$

where $\boldsymbol{C}_{\boldsymbol{mh}}$, $\boldsymbol{C}_{\boldsymbol{hh}}$, and $\boldsymbol{C}_{\boldsymbol{vv}}$ are covariance matrices calculated over the ensemble of $\boldsymbol{m}_{s,k+1|k}$, $\boldsymbol{h}_{s,k+1|k}$, and $\boldsymbol{v}_{k+1}$, respectively. In the filtering step, each member of the statistical ensemble of $\boldsymbol{m}_{s,k+1}$ is updated according to

$$\boldsymbol{m}^r_{s,k+1} = \boldsymbol{m}^r_{s,k+1|k} + \boldsymbol{K}_{s,k+1}(\boldsymbol{z}^r_{s,k+1} - \boldsymbol{h}^r_{s,k+1|k}), \tag{2.6}$$

where $\boldsymbol{z}^r_{s,k+1}$ is formed as follows [17]:

$$\boldsymbol{z}^r_{s,k+1} = \boldsymbol{z}_{s,k+1} + \boldsymbol{v}^r_{s,k+1} \tag{2.7}$$

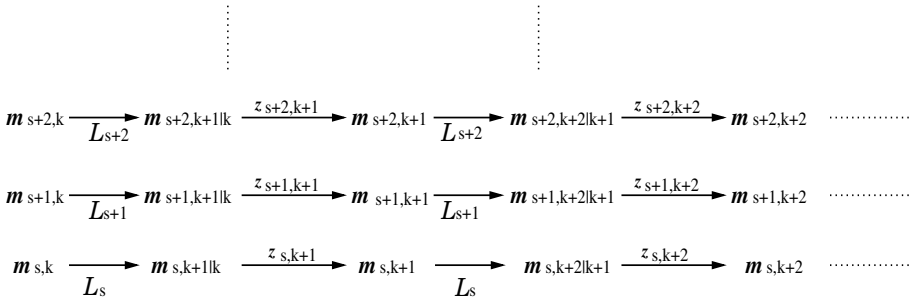

FIG. 2.1. *Multiscale EnKF data assimilation with models and observations given in all scales.*

and can be interpreted as the rth member from a statistical ensemble of observations with mean equal to the physical observation $\boldsymbol{z}_{s,k+1}$ at time $k+1$. Moreover, in addition to being temporally independent, the vector $\boldsymbol{v}^r_{s,k+1}$ representing the observation model error is assumed to have a diagonal covariance matrix. The data assimilation in this case can be illustrated by Figure 2.1, where the present scheme, in which information at a given scale is assimilated only by states at that scale, yields predictions and updating in different scales that are actually independent of each other.

2.2. Data assimilation with interscale coupling. In many cases of interest, however, the explicit system model and observation may not be available simultaneously at some scales. In these cases, the model state at some scale of interest may still need to be updated by measurements from some other scale. This is actually a problem of inverse analysis if the state of the model associated with the information-rich scale is used to determine the state of a model associated with a coarser scale. In this case, multiscale bridging models that are used to relate model states associated with different scales are clearly needed. These are developed in the next section. For now, suppose the bridging model between two adjacent scales, s and $s+1$, is given by

$$\boldsymbol{m}_{s+1,k} = \mathcal{F}_{s+1,s}(\boldsymbol{m}_{s,k}). \tag{2.8}$$

Combined with (2.1), an augmented equation is written as

$$\begin{cases} \boldsymbol{m}_{s+1,k+1} = \mathcal{F}_{s+1,s}(\mathcal{L}_s(\boldsymbol{m}_{s,k})), \\ \boldsymbol{m}_{s,k+1} = \mathcal{L}_s(\boldsymbol{m}_{s,k}), \end{cases} \tag{2.9}$$

which can be rewritten as

$$\boldsymbol{M}_{s,k+1} = \mathcal{L}^*_s(\boldsymbol{m}_{s,k}), \tag{2.10}$$

where

$$\boldsymbol{M}_{s,k+1} = \begin{Bmatrix} \boldsymbol{m}_{s+1,k+1} \\ \boldsymbol{m}_{s,k+1} \end{Bmatrix}.$$

Together with the rewritten form of (2.2),

$$\boldsymbol{z}_{s+1,k+1} = \mathcal{H}^*_{s+1}(\boldsymbol{M}_{s,k+1}) + \boldsymbol{v}^*_{s+1,k+1}, \tag{2.11}$$

the updated model state $\boldsymbol{m}_{s,k+1}$ can be obtained by the aforementioned EnKF procedures using the coarser-scale measurement $\boldsymbol{z}_{s+1,k+1}$. The coarser-scale model state

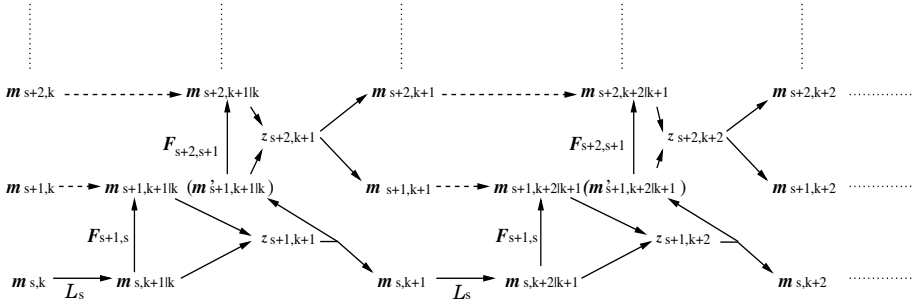

FIG. 2.2. *Multiscale EnKF data assimilation with observations or explicit models absent in some scales.*

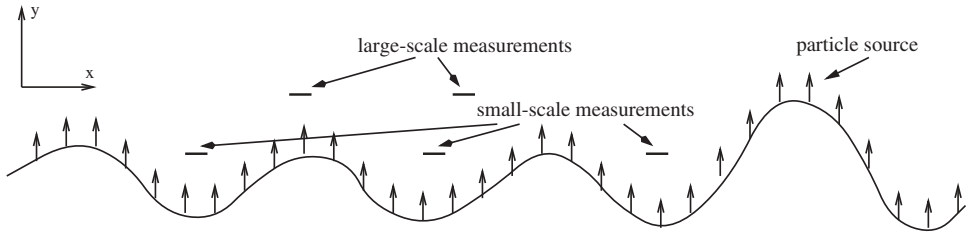

FIG. 2.3. *Particle source in a one-dimensional continuous boundary and measurements in different scales.*

$\boldsymbol{m}_{s+1,k+1}$ is also updated at the same time, which means that the model state in a given scale can still be updated even if the system model is not explicitly observable at that scale.

If a measurement of an even coarser scale, $\boldsymbol{z}_{s+2,k+1}$, can be observed, the updated model state in scale $s+1$, $\boldsymbol{m}_{s+1,k+1}$, can be taken as the predicted model state, $\boldsymbol{m}'_{s+1,k+1|k}$, in that scale and the EnKF used to compute a newly updated $\boldsymbol{m}_{s+1,k+1}$ based on $\boldsymbol{z}_{s+2,k+1}$. The model state in scale $s+2$ is also updated in this procedure.

Notice that when the model state $\boldsymbol{m}_{s+1,k+1}$ updated by $\boldsymbol{z}_{s+1,k+1}$ is taken as the predicted state, $\boldsymbol{m}'_{s+1,k+1|k}$, waiting for the updating of $\boldsymbol{z}_{s+2,k+1}$, $\boldsymbol{m}'_{s+1,k+1|k}$ can be viewed as a forecast obtained from $\boldsymbol{m}_{s+1,k}$ by a more accurate system model in scale $s+1$, which is obtained by calibration of the measurement $\boldsymbol{z}_{s+1,k+1}$ but which cannot be explicitly expressed. Following this idea, model states in different scales can be updated for the cases that the observations are not available in some scales but the explicit or implicit system models in these scales are known and observations at the coarser scale are available. This procedure is also valuable for cases where system models are not explicitly available in some scales but the measurements in these scales are accessible and explicit or implicit system models at the finer scale are known. The multiscale EnKF data assimilation in these cases can thus be illustrated by Figure 2.2.

To estimate the particle fluxes in different scales above a boundary, particle fluxes can be taken as the model state, $\boldsymbol{m}_{s,k}$, and the lowest-scale evolution model for $\boldsymbol{m}_{1,k}$ needs to be specified. Instruments are laid out at intervals in coarser scales to measure the fluxes of particles across these intervals, as illustrated in Figure 2.3. Using the multiscale EnKF data assimilation approach described above, measurements from these instruments are assimilated with the model predictions to obtain the estimates

of fluxes in different scales.

The above analysis indicates that the multiscale bridging model is very important for the implementation of the multiscale EnKF data assimilation method. Therefore, in order to apply this approach to estimate the boundary particle fluxes, a bridging model has to be devised to relate fluxes in different scales above the boundary. This is achieved in the following two sections.

3. Probabilistic model for typical boundaries emitting particles with transverse random walk. Suppose that there are point sources along a continuous boundary and particles are emitted from the sources in the upward vertical direction, as illustrated in Figure 2.3. The particle fluxes form a random process, which obeys specified statistics over space and time. Each particle has a constant velocity V and moves with random walk in the transverse direction. The dynamic interaction between particles is assumed negligible, and the particle flow is assumed to be in a steady state. With these assumptions, and neglecting gravity, the equations governing the motion of particles in the horizontal and vertical directions are given by

$$dx = Ddw, \tag{3.1}$$

$$y = Vt + y_0, \tag{3.2}$$

where D is the diffusion coefficient of particles, $w(t)$ a Wiener process [4], and y_0 the initial position of particles in the y-direction. Here the particle velocity in the vertical direction is assumed to be much greater than the diffusion effect of Brownian motion in that direction. Thus, Brownian motion in the y-direction is neglected.

The Fokker–Planck equation for the stochastic differential equation (3.1) can be stated as [16]

$$\frac{\partial p}{\partial t} = \frac{D^2}{2}\frac{\partial^2 p}{\partial x^2}, \tag{3.3}$$

where $p(x,t)$ is the probability density function (p.d.f.) of a particle existing at location x at time t. The above equation can be written in the following form when (3.2) is considered:

$$\frac{\partial p}{\partial y} = \frac{D^2}{2V}\frac{\partial^2 p}{\partial x^2}. \tag{3.4}$$

This equation can be used to calculate the probability of a particle across a transverse length interval (x_{j-1}, x_j) at a fixed distance h above a source at a_i in a plain boundary. This quantity is a building block in the multiscale approach for calculating particle fluxes in different scales. Its functional form depends on the specific boundary conditions imposed on the particle fluxes. In particular, three types of such boundary conditions are considered next, as they affect the upward migration of particles.

Case 1. The plain boundary without vertical barriers (Figure 3.1).

Given the initial condition $p(x,0) = \delta(x - a_i)$, the solution of (3.4) is expressed as [9]

$$p_0(x,y) = \frac{1}{(2\pi D^2 y/V)^{1/2}} e^{-\frac{(x-a_i)^2}{2D^2 y/V}}. \tag{3.5}$$

Therefore, the probability that the particle falls within the length interval (x_{j-1}, x_j) at h can be obtained as

$$P_0(i,j,h) = \int_{x_{j-1}}^{x_j} p_0(x,h)dx = \int_{x_{j-1}-a_i}^{x_j-a_i} \frac{1}{(2\pi D^2 h/V)^{1/2}} e^{-\frac{x^2}{2D^2 h/V}} dx. \tag{3.6}$$

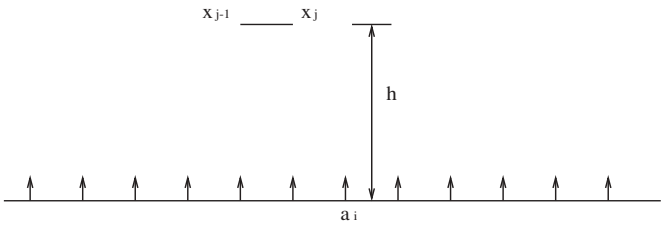

FIG. 3.1. *The plain boundary without vertical barriers.*

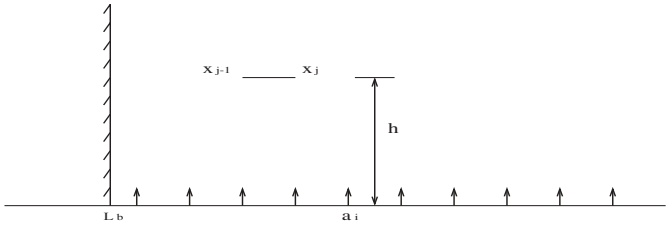

FIG. 3.2. *The plain boundary with one vertical barrier.*

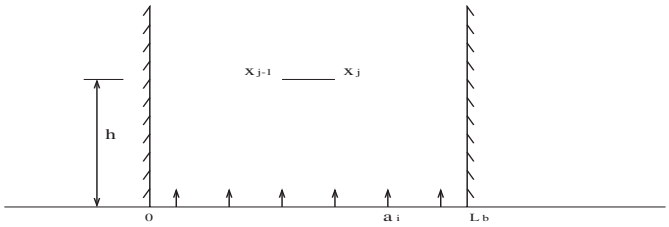

FIG. 3.3. *The plain boundary with two vertical barriers.*

Case 2. The plain boundary with a one-sided vertical absorbing barrier (Figure 3.2).

If a vertical absorbing barrier exists at the location L_b in the boundary, a boundary condition for (3.4) of the form $p(L_b, y) = 0$ must be added to the initial condition, and the solution is therefore given by [9]

$$p_1(x,y) = p_0(x,y) - p_0(2L_b - x, y), \quad x \geq L_b, \quad a_i \geq L_b, \tag{3.7}$$

and

$$P_1(i,j,h) = \int_{x_{j-1}}^{x_j} p_1(x,h)dx, \tag{3.8}$$

where $x_{j-1}, x_j > L_b$.

Case 3. The plain boundary with two-sided vertical absorbing barriers (Figure 3.3).

In the case where two vertical absorbing barriers exist at both sides of a point source, the boundary conditions change to $p(0,y) = 0$ and $p(L_b, y) = 0$. The solution is obtained by the classical method of separation of variables [9], resulting in

$$p_2(x,y) = \sum_{n=1}^{\infty} \frac{2}{L_b} \sin\left(\frac{n\pi a_i}{L_b}\right) \sin\left(\frac{n\pi x}{L_b}\right) e^{-\frac{D^2}{2V}\frac{n^2\pi^2 y}{L_b^2}} \tag{3.9}$$

and

$$P_2(i,j,h) = \int_{x_{j-1}}^{x_j} p_2(x,h)dx$$
$$= -\sum_{n=1}^{\infty} \frac{2}{n\pi} \sin\left(\frac{n\pi a_i}{L_b}\right) e^{-\frac{D^2}{2V}\frac{n^2\pi^2 h}{L_b^2}} \cos\left(\frac{n\pi x}{L_b}\right)\Big|_{x_{j-1}}^{x_j}, \tag{3.10}$$

where $0 < x_{j-1}, x_j < L_b$.

4. Multiscale bridging model for particle fluxes in boundaries with arbitrary profiles. In most problems of interest, boundary profiles, while different from the three standard conditions considered in the previous section, can be recovered from them through a limiting process as presented in this section. Also, while the present investigation is limited to the one-dimensional case (Figure 2.3), it can be readily generalized to two-dimensional surfaces.

Similarly to the above analysis, particles are assumed to be emitted vertically from the boundary and reaching their steady state almost instantly. Moreover, boundaries are assumed to be absorbing; i.e., particles contacting the boundary during their motion have a zero probability of reentering the flow. Based on these assumptions the absorbed particles incoming from the above domain are independent from the particles emitted from the boundary. These emitted particles do not represent reflected incoming particles but are rather released by some specific source, such as vegetation along the boundary. The p.d.f. for the position of a particle emitted from a source at location a along the boundary can be computed as the solution to

$$\frac{\partial p}{\partial y} = \frac{D^2}{2V}\frac{\partial^2 p}{\partial x^2}, \quad p(x, g(x)) = \delta(x-a), \tag{4.1}$$

where $y = g(x)$ is the function representing the boundary shape and $(a, g(a))$ is the coordinate of the point source.

The above model is actually a typical moving-boundary problem for the diffusion equation. To solve this problem, a multiscale approach is developed that relies on the results from the previous section.

Since the boundary possesses an arbitrary profile, to calculate the probability of particles from a point source arriving at a coarser-scale interval, the boundary is discretized using a structured mesh, and particles are assumed to be released from the point in the meshed boundary which has the same x-coordinate as the original point, as shown in Figure 4.1. The meshed boundary is chosen such that for the descending (respectively, ascending) part of the true boundary, the right-end (respectively, left-end) points of its horizontal segments are the nearest mesh grids below the true boundary. It is noted that only the case where particles are released from a point inside the flat part of the boundary is indicated in Figure 4.1. This is justified later in this section. The meshed boundary can be viewed as enveloping a hierarchy of virtual boundaries with increasing flatness. Each virtual boundary comprises a meshed lower side and two adjacent walls whose horizontal segments are meshed. These virtual boundaries play the role of intermediate scales necessitated by the numerical propagation of observables from the microscale (lowermost boundary) to the macroscale (uppermost boundary). Since particle fluxes cross only the bottom of each of these intermediate scales, they each can be represented by its meshed lower side. In the following, the word *scale* will refer to the meshed lower side of each intermediate scale, while the lower and upper bounds of the meshed domain will be referred to as the

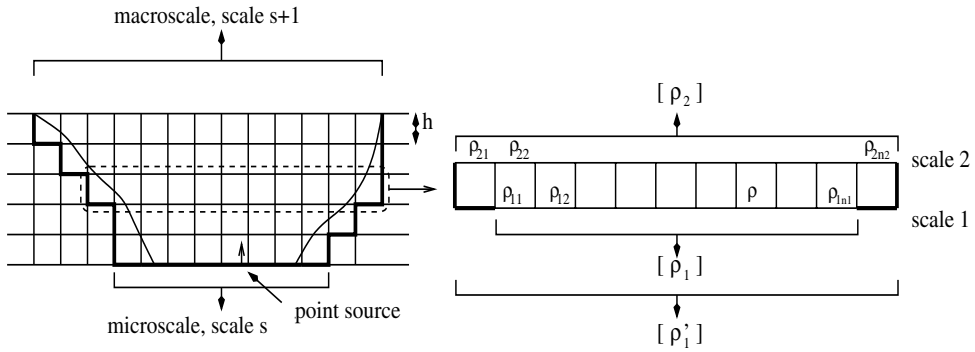

FIG. 4.1. *Illustration for discretization and different scales.*

microscale and macroscale, respectively. As the mesh size decreases, the macroscale and microscale gradually approach the true upper and lower bounds, and the meshed boundary approaches the true boundary.

The probability of a particle reaching any given interval in a coarse scale is obtained from those probabilities at the adjacent smaller scale, using the results in section 3. Specifically, consider the meshed boundary shape shown in Figure 4.1. Let the probability of a particle crossing interval i at scale 1 be denoted by ρ_{1i}, $i = 1, 2, \ldots, n_1$, where n_1 is the number of mesh cells at scale 1, and let the vector $[\rho_1']$ be given by

$$[\rho_1'] = [\underbrace{0, \ldots, 0}_{s_1\ 0\text{'s}}, \rho_{11}, \ldots, \rho_{1n_1}, \underbrace{0, \ldots, 0}_{s_2\ 0\text{'s}}]^T, \tag{4.2}$$

where s_1 and s_2 are the numbers of extruding mesh cells, to the left and to the right, respectively, at scale 2 beyond the projection of scale 1 on scale 2. If n_2 denotes the numbers of mesh cells at scale 2, then, clearly, $n_2 = n_1 + s_1 + s_2$.

Consequently, assuming that the probability of a particle crossing any given cell in the spatial partition of scale 1 is accumulated at the midpoint of this cell, the probability of a particle crossing any of the n_2 intervals at scale 2 can be obtained as

$$[\rho_2] = [M]^T[\rho_1'], \tag{4.3}$$

where $[\rho_2]$ is a vector formed by ρ_{2j}, $j = 1, 2, \ldots, n_2$, and the component of $[M]$, $[M]_{ij} = P_2(i, j, h)$, where h denotes the mesh size and P_2 is given by (3.10).

Given (3.10) and (4.3), the probability of a particle arriving at any interval at a particular scale can be calculated for the meshed boundary in Figure 4.1. Equation (3.10) also applies to the boundary with one-sided absorbing walls and the boundary with no vertical barriers. For the latter, the discretization provided by (3.10) is not necessary, as the interscale transition probability can be directly obtained from (3.6). For the boundary with a one-sided wall, (3.8) is of no practical use, as the probabilities have to be calculated over a semi-infinite domain. In this case, the probabilities in the domain at a large distance from the particle sources can be assumed to be zero, and the computation may be limited to a finite domain which is obtained by truncating the semi-infinite domain using an imaginary vertical absorbing wall. Therefore, (3.10) can be applied. It should be noted that the probability of a particle arriving at intervals at a particular scale should converge as the mesh size decreases.

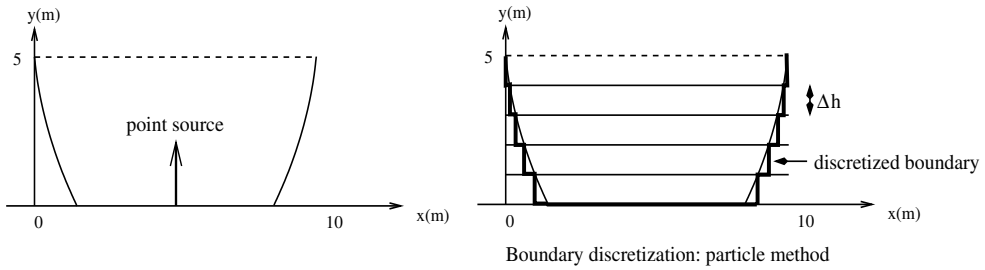

FIG. 4.2. *A symmetric one-dimensional boundary with parabolic walls.*

To validate the proposed approach, it is compared with the particle method which directly traces the trajectory of each particle. For that, consider a symmetric one-dimensional boundary with two-sided parabolic absorbing walls (Figure 4.2):

$$y = \begin{cases} 0.4(x-5)^2 - 5(m) & \text{if } 0 < x < 5 - \frac{5}{2}\sqrt{2}(m), \\ 0 & \text{if } 5 - \frac{5}{2}\sqrt{2} < x < 5 + \frac{5}{2}\sqrt{2}(m), \\ 0.4(x-5)^2 - 5(m) & \text{if } 5 + \frac{5}{2}\sqrt{2} < x < 10(m). \end{cases}$$

The particle source is located on the boundary at coordinates $(x, y) = (5m, 0)$. For the particle method, 10000 identical particles with transverse Brownian motion are released to evaluate the probability that one particle emitted from the source will be able to arrive at the upper bound of the boundary. The size of the time step, dt, used to compute the particle positions in (3.1) and (3.2) is defined as $dt = \Delta h/V$, where Δh is the mesh size used to discretize the boundary (see Figure 4.2) and V is the velocity of particles. It is noted that the discretization of the boundary in the particle method is different from that in the multiscale method, as indicated in Figure 4.2. At every time step, those particles located outside the discretized boundary are removed from the computation, and the number of particles eventually reaching the upper bound, N_u, is counted. The probability is calculated as the ratio of N_u to 10000. For both methods, the diffusion coefficient D and velocity V are taken as $5.0cm/s^{1/2}$ and $0.2cm/s$, respectively. Results from the two methods are plotted in Figure 4.3, which indicates that both methods give almost identical converged results as the mesh size decreases. The multiscale method presented above achieves similar convergence to the particle method at a much coarser spatial discretization.

An important issue that needs to be clarified is that only Brownian particles released from the horizontal flat part of a boundary can arrive at upper scales. Particles emitted from the curved part of the boundary cannot escape arbitrarily small vicinities around the source. This statement can be easily verified by observing that the boundary can be truncated, without affecting the dynamics of the emitted particles, by a horizontal line crossing the source point (Figure 4.4). Since the multiscale method is valid for computing the probability of particles arriving at upper scales, it can be used to obtain the results for the case shown in Figure 4.4. However, as the mesh size for discretization is reduced, the rightmost vertical side of the bottom mesh will approach the point source. Thus, with reference to (3.10), as $h \to 0$, $L_b \to a_i$. In the limit, as $h \to 0$, $P_2(i, j, h) \to 0$, indicating that particles with transverse Brownian motion have a zero probability of escaping the curved part of the boundary.

For a continuous source along the flat part of a boundary, the boundary is first discretized using a particular mesh size. The particles emitted within a mesh cell in

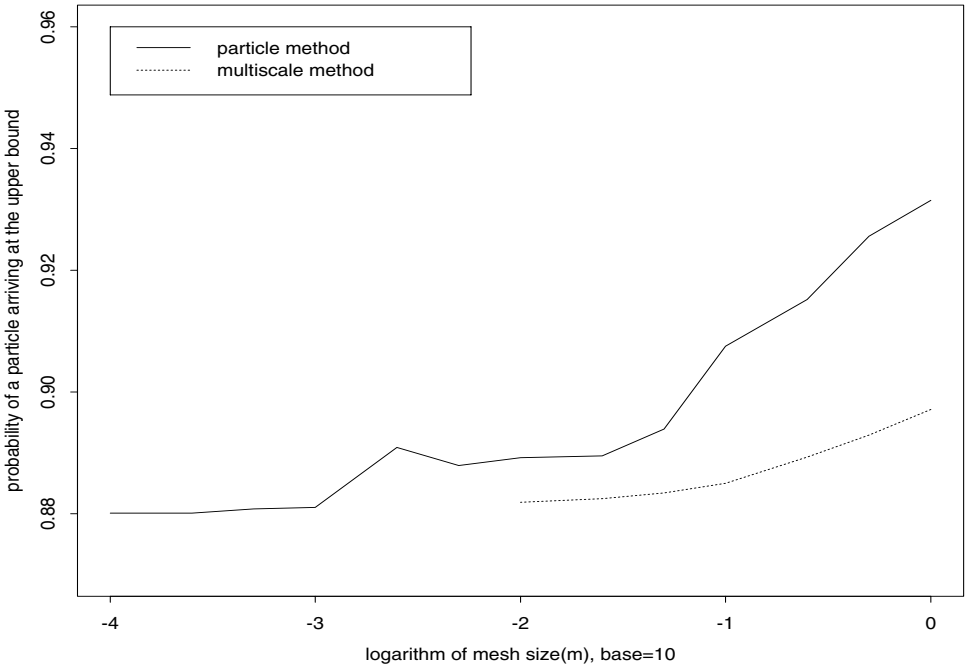

FIG. 4.3. *Comparison between the particle method and multiscale method.*

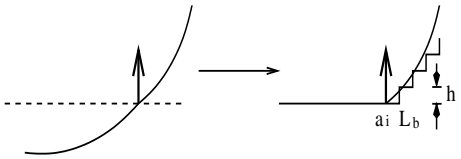

FIG. 4.4. *Particle source located in a curve boundary.*

the microscale of the meshed boundary are assumed to be released from the midpoint of this mesh cell. Then the probabilities of particles, which are emitted from the midpoints of mesh cells in the microscale, arriving at mesh cells in the macroscale can be computed. In the following, the microscale and the macroscale will be denoted as s and $s+1$, respectively (Figure 4.1). Suppose that the numbers of mesh cells in the micro- and macroscale are n_s and n_{s+1}, respectively, and that the probability of particles, emitted from the ith mesh cell in scale s, arriving at the jth mesh cell in scale $s+1$ is computed as $\lambda_{i,j}$, $i = 1, \ldots, n_s$, $j = 1, \ldots, n_{s+1}$. Then the joint probability that $f_{i,j}$ particles, out of $\boldsymbol{M}_s(i)$ particles from the ith mesh cell in scale s, arrive at the jth mesh cell in scale $s+1$ can be obtained from the multinomial distribution

$$p(f_{i,1}, f_{i,2}, \ldots, f_{i,n_{s+1}}) = \frac{\boldsymbol{M}_s(i)!}{f_{i,1}! f_{i,2}! \ldots f_{i,n_{s+1}}! (\boldsymbol{M}_s(i) - \sum_{j=1}^{n_{s+1}} f_{i,j})!} \cdot \prod_{j=1}^{n_{s+1}} \lambda_{i,j}^{f_{i,j}} \left(1 - \sum_{j=1}^{n_{s+1}} \lambda_{i,j}\right)^{\boldsymbol{M}_s(i) - \sum_{j=1}^{n_{s+1}} f_{i,j}}, \tag{4.4}$$

where $\boldsymbol{M}_s(i) = \text{int}(\boldsymbol{m}_s(i)\Delta m\Delta t)$ and $\boldsymbol{m}_s(i)$ is the value of particle fluxes at the midpoint of the ith mesh cell in scale s. The operator $\text{int}(\cdot)$ stands for the maximum integer less than the value in the parenthesis.

The value of particle flux at the midpoint of the jth mesh cell in scale $s+1$ can thus be obtained as

$$\boldsymbol{m}_{s+1}(j) = \boldsymbol{M}_{s+1}(j)/(\Delta m\Delta t) = \sum_{i=1}^{n_s} f_{i,j}/(\Delta m\Delta t), \tag{4.5}$$

where Δm and Δt stand for the mesh size and time interval, respectively.

As the mesh size decreases, the particle fluxes in scale $s+1$ should converge to their true distribution. Hence, for each realization of the process, $\boldsymbol{m}_s$, a corresponding realization of the process, $\boldsymbol{m}_{s+1}$, can be computed. A multiscale bridging model relating the flux processes of two different scales, i.e., the operator $\mathcal{F}_{s+1,s}(\cdot)$ in (2.8), is thus constructed.

5. Numerical simulations and result analyses. Since in most applications the irregular boundaries are very thin compared with LES computational domains above them, particles incoming from the LES domain and crossing the imaginary macroscale boundary are assumed to come in contact with the irregular absorbing microscale boundary. Hence, the macroscale boundary can also be viewed as absorbing, and the particles emitted by it are only those released by the microscale boundary. Therefore, to obtain appropriate particle fluxes across the macroscale boundary and into LES computational domains, it is necessary to estimate only fluxes of particles emitted from the microscale boundary.

To evaluate the effect of the proposed multiscale EnKF data assimilation approach on boundary flux estimation, a boundary profile, which is generated by replicating the truncated parabolic function

$$y = \begin{cases} \frac{10}{9}(x-0.5)^2 - \frac{8}{45}(m) & \text{if } 0 < x < 0.1(m), \\ 0 & \text{if } 0.1 < x < 0.9(m), \\ \frac{10}{9}(x-0.5)^2 - \frac{8}{45}(m) & \text{if } 0.9 < x < 1.0(m) \end{cases}$$

to eight adjacent positions (Figure 5.1), is used. Each shape element (a truncated parabolic form) contains continuous sources at the bottom. In this example, we estimate only the particle fluxes across the bottom boundary and upper boundary at $y = 0.1m$ (referred to as microscale and macroscale fluxes, respectively). Hence, only two scales are used in the multiscale EnKF approach. This two-scale example can be used as a template in constructing the estimation scheme across many scales.

The true microscale particle fluxes are assumed to be constant in the time domain. Therefore, for this example, the operator, $\mathcal{L}_s(\cdot)$, in the microscale system model is an identity matrix, $I_{8N_s\times 8N_s}$, where N_s is the number of mesh cells at the microscale of each shape element. A stationary bandlimited white-noise Gaussian random process is used to describe initial microscale particle fluxes at the boundary bottom (Figure 5.1), and accordingly an ensemble of initial realizations of microscale particle fluxes, which correspond to $\boldsymbol{m}_{s,0}^r \in \mathbb{R}^{8N_s}$, $r = 1, \ldots, N_e$, in (2.3), are generated using the spectral method [15]. The initial guess for the mean value of the random process is set to $400s^{-1}cm^{-1}$, while the initial error spectral density function is plotted in Figure 5.2. It is noted that the errors in the EnKF also represent the fluctuations conditioned on the a priori information.

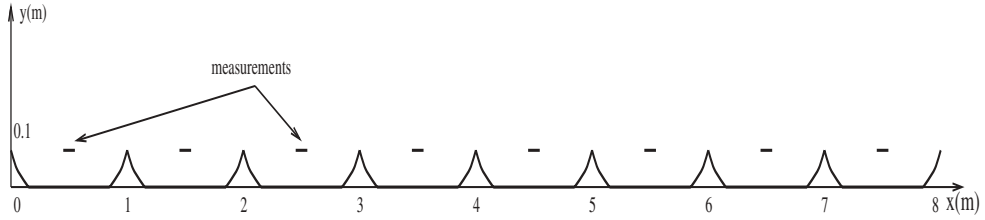

FIG. 5.1. *The boundary profile for numerical simulations.*

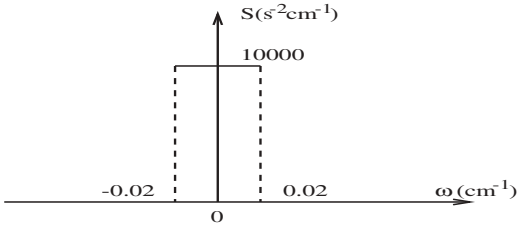

FIG. 5.2. *Initial guess for the error spectral density function of the boundary microscale fluxes.*

For each realization of predicted microscale particle fluxes, $\boldsymbol{m}^r_{s,k+1|k}$, the corresponding predicted macroscale fluxes, $\boldsymbol{m}^r_{s+1,k+1|k}$, can be computed using the bridging operator $\mathcal{F}_{s+1,s} : \mathbb{R}^{8N_s} \mapsto \mathbb{R}^{8N_{s+1}}$, which is constructed in the previous section. To compute the macroscale fluxes, the microscale particle fluxes, the diffusion coefficient D, and the particle velocity V need to be known. The latter two parameters are both microscale quantities, and hence can also be included in the microscale state $\boldsymbol{m}_s$ and estimated by the multiscale data assimilation method. Here, for simplicity, these two parameters are assumed to be available a priori.

As shown in Figure 5.1, eight instruments with an identical length, 8cm, are placed at midpoints of eight macroscale patches to measure the particle fluxes across the intervals covered by these instruments. The observation values at the measurement locations at each time step $\boldsymbol{z}_{s+1,k+1}$ are computed assuming that the true microscale flux for the continuous source is a constant of $500s^{-1}cm^{-1}$ over the space and time domain. The operator $\mathcal{H}^*_{s+1}(\cdot)$ in (2.11) is a mapping $\mathbb{R}^{8(N_s+N_{s+1})} \mapsto \mathbb{R}^8$, and each realization of predicted values of the observation, $\boldsymbol{h}^{*r}_{s+1,k+1|k} = \mathcal{H}^*_{s+1}(\boldsymbol{M}^r_{s,k+1|k})$, can be easily obtained by computing macroscale particle fluxes across intervals covered by the eight instruments.

Each term in the Kalman gain matrix in (2.5) is obtained as follows:

$$\boldsymbol{C}_{\boldsymbol{mh}} = \left(\sum_{r=1}^{N_e} (\boldsymbol{M}^r_{s,k+1|k} - \bar{\boldsymbol{M}}_{s,k+1|k})(\boldsymbol{h}^{*r}_{s+1,k+1|k} - \bar{\boldsymbol{h}}^*_{s+1,k+1|k})^T \right) \Big/ N_e,$$

$$\boldsymbol{C}_{\boldsymbol{hh}} = \left(\sum_{r=1}^{N_e} (\boldsymbol{h}^{*r}_{s+1,k+1|k} - \bar{\boldsymbol{h}}^*_{s+1,k+1|k})(\boldsymbol{h}^{*r}_{s+1,k+1|k} - \bar{\boldsymbol{h}}^*_{s+1,k+1|k})^T \right) \Big/ N_e,$$

$$\boldsymbol{C}_{\boldsymbol{vv}} = R_{\boldsymbol{v}} I_{8\times 8}, \tag{5.1}$$

TABLE 1
Parameters in the numerical simulations.

Ensemble size	500, 2000
Mesh size (cm)	2.0, 1.0, 0.5
Var. of measurement error	10.0
Diffusion coef. D (cm/s $^{1/2}$)	2.0
Particle velocity V(cm/s)	0.2
Time interval (s)	1.0

where $R_{\boldsymbol{v}}$ is the variance of measurement error, I is an identity matrix, and

$$\bar{\boldsymbol{M}}_{s,k+1|k} = \sum_{r=1}^{N_e} \boldsymbol{M}^r_{s,k+1|k}/N_e,$$

$$\bar{\boldsymbol{h}}^*_{s+1,k+1|k} = \sum_{r=1}^{N_e} \boldsymbol{h}^{*r}_{s+1,k+1|k}/N_e.$$

Different mesh sizes are used to discretize the boundary. Statistical properties, such as the mean value and error covariance of particle fluxes crossing the micro- and macroscale, are calculated from the ensemble. Parameters in the simulations, such as the variance of measurement error, diffusion coefficient, particle velocity, ensemble size, and mesh size, are listed in Table 1. It is noted that the ensemble size has a very small effect on the statistical properties of fluxes before and after the filtering; thus only the case where the ensemble size $N_e = 500$ is plotted.

At the beginning of estimation, the filtering is made only at the first time step so that effects of the mesh size on the updating of statistics of fluxes can be examined. The statistics of fluxes before and after calibration are calculated and plotted in Figures 5.3–5.6.

The estimates of microscale and macroscale fluxes are plotted in Figure 5.3 and Figure 5.5, respectively. Since the measurement values are all larger than the predicted particle fluxes across the measurement intervals, the estimates of microscale and macroscale fluxes are all increased along the boundary after updating. In Figure 5.3, the updated estimates of microscale particle fluxes have very similar spatial configurations for mesh sizes of 2cm, 1cm, and 0.5cm. In Figure 5.5, there are two clusters of estimates of macroscale particle fluxes, of which the lower one contains the estimates prior to the updating and the upper one the estimates after assimilation. In each cluster, the estimates almost coincide for different mesh sizes.

The fluctuating parts of the updated microscale fluxes are assumed to be stationary with zero mean. The associated error covariances of fluxes are plotted in Figure 5.4. The error covariances of the macroscale fluxes are directly computed without the assumption of stationarity, and curves for the error covariances $Cov(0.5m, x)$, $x \geq 0.5m$, are compared for different mesh sizes in Figure 5.6. As can be seen in the two figures, the variances of micro- and macroscale fluxes are both reduced because the measurements are informative to the model predictions. Similar to the observations in Figure 5.3, updated variances are almost the same for different mesh sizes in Figure 5.4. In Figure 5.6, the covariance curves prior to updating are clustered (cluster A) and exhibit strong correlation. The covariance curves following updating are also clustered (cluster B) with a much diminished correlation. It can be seen

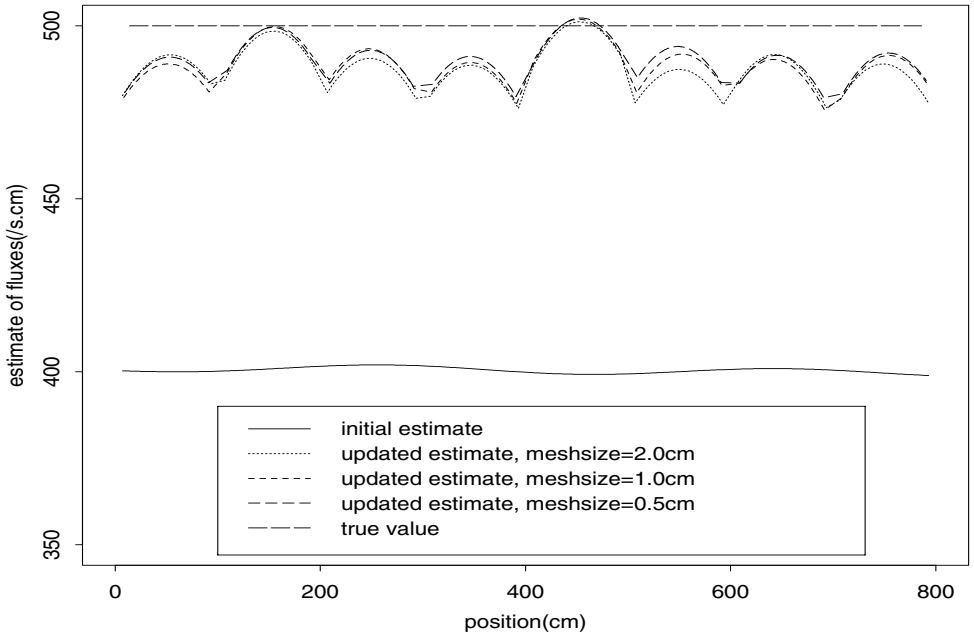

FIG. 5.3. *Estimates of the microscale fluxes;* $N_e = 500$.

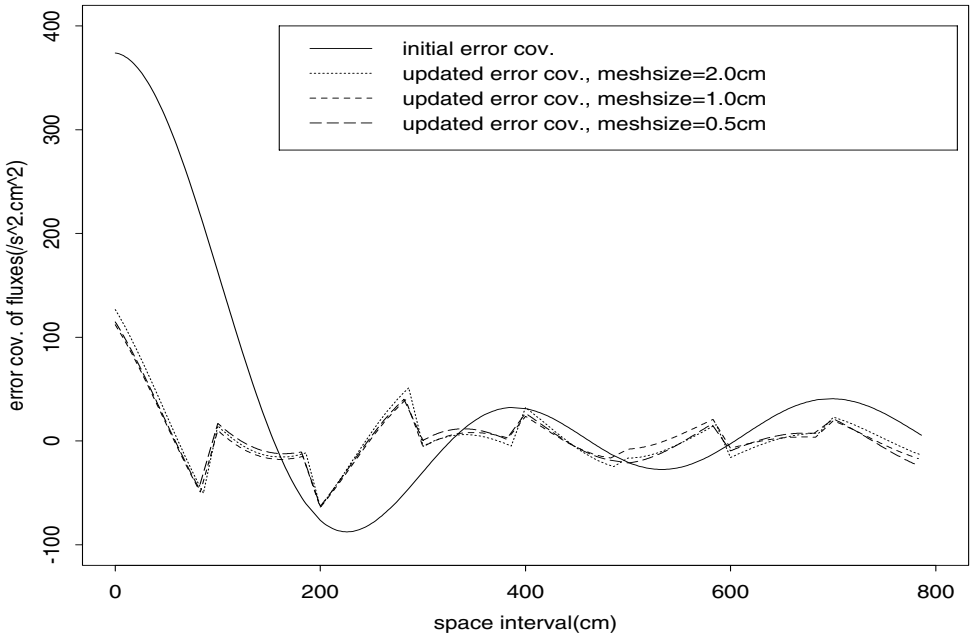

FIG. 5.4. *Error covariances of the microscale fluxes;* $N_e = 500$.

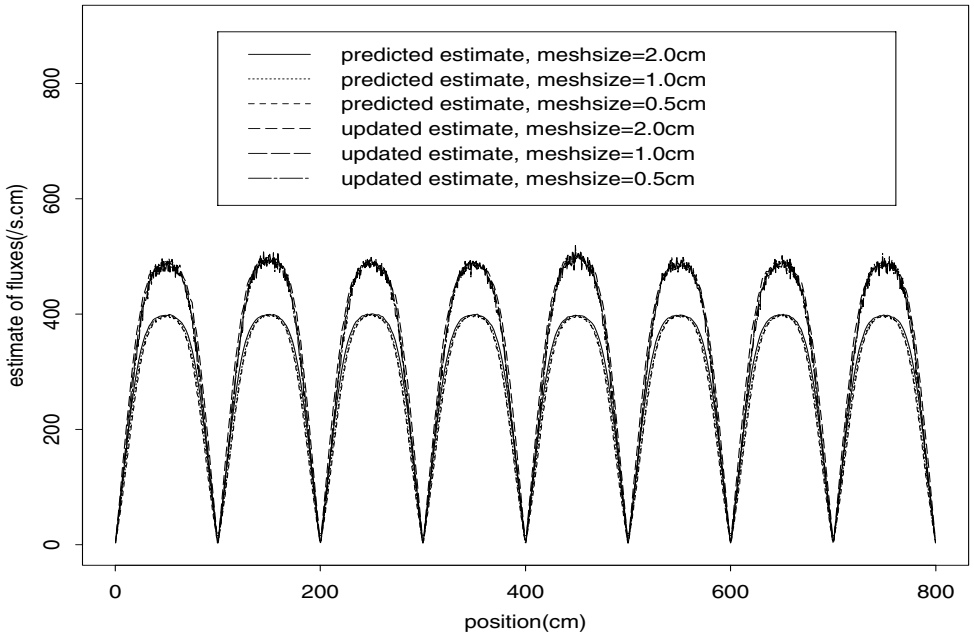

FIG. 5.5. *Estimates of the macroscale fluxes;* $N_e = 500$.

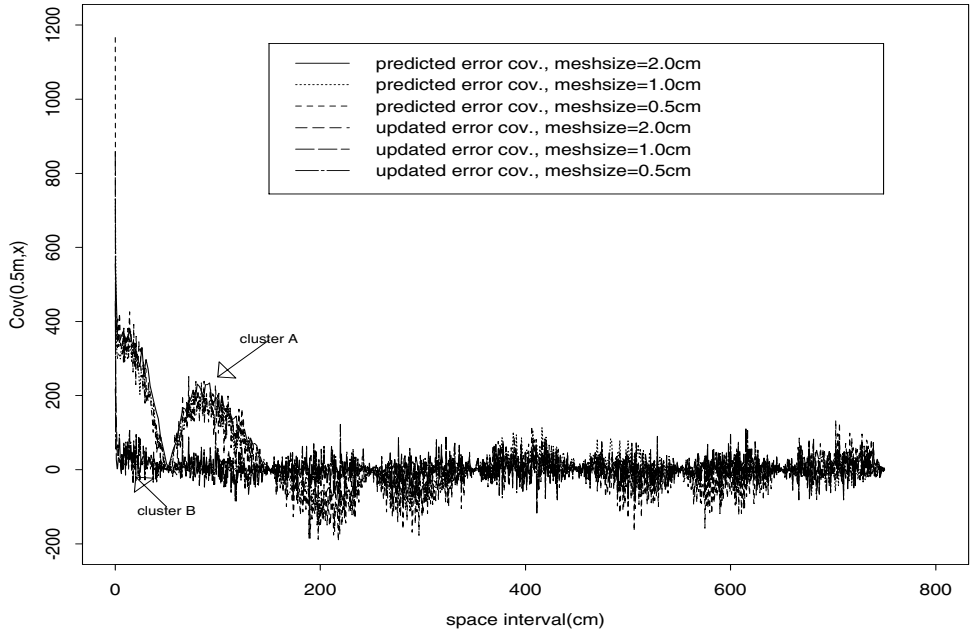

FIG. 5.6. *Comparison of error covariances* $Cov(0.5, x)$, $x \geq 0.5m$, *of the macroscale fluxes;* $N_e = 500$.

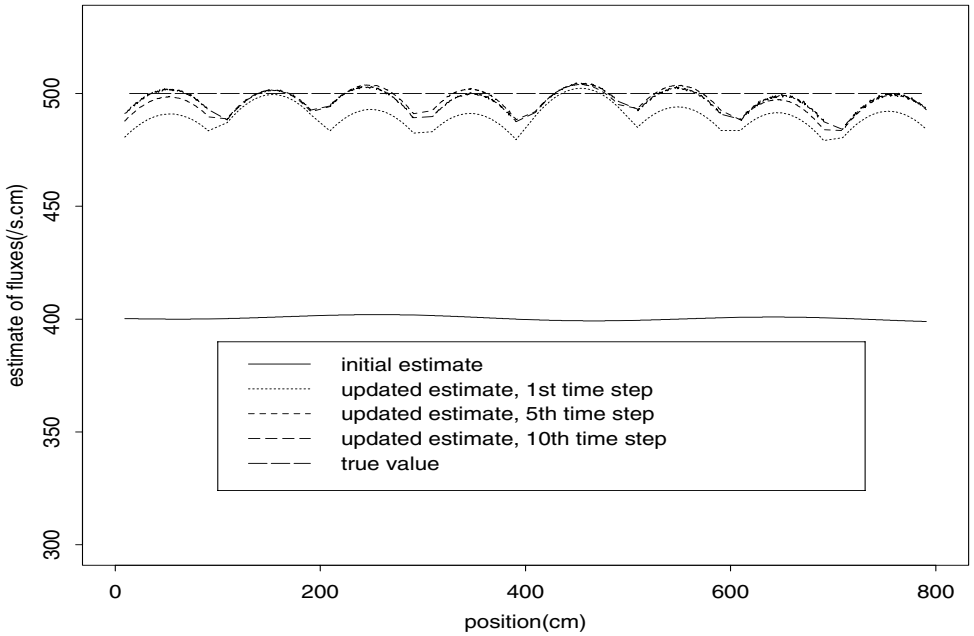

FIG. 5.7. *Updated estimates of microscale fluxes at different time steps;* $N_e = 500$*; mesh size* $= 0.5cm$.

that curves in each cluster are very similar for different mesh sizes. Therefore, it can be concluded that estimates and error covariances of microscale and macroscale fluxes converge very rapidly as the mesh size is decreased. As the mesh size equals 0.5cm, these statistics are almost converged. It is again noted that in the context of the EnKF the error covariances of the estimated states are in fact the conditional covariances of these states and can therefore be construed as useful statistics.

Based on the observations of the above preliminary estimation, an ensemble size 500 and mesh size 0.5cm are used to complete the filtering procedure. Here, the estimates and error covariances of particle fluxes are calibrated at 10 successive time steps, and the results at some time steps are plotted in Figures 5.7–5.11. Figure 5.7 shows that the updated estimates of microscale particle fluxes converge to the true constant value as the time proceeds. In Figure 5.8, the updated error covariances of microscale fluxes almost converge to the true value, which is a constant covariance of zero. Updated estimates of macroscale fluxes are plotted in Figure 5.9. It can be seen that these estimates at different time steps are very close to the true mean value, which is computed by assuming the true microscale fluxes are a constant of $500s^{-1}cm^{-1}$ over the space and time domain. Curves for the covariances $Cov(0.5m, x)$, $x \geq 0.5m$, of the updated macroscale fluxes are compared in Figure 5.10, and they all agree well with the true covariance of macroscale fluxes. The differences between these curves and the true covariance are shown in Figure 5.11, which indicates that these differences are very small when compared with the true variance. All these results show that the statistics of macroscale and microscale fluxes converge very rapidly to the true statistics as the filtering procedure proceeds in the time domain.

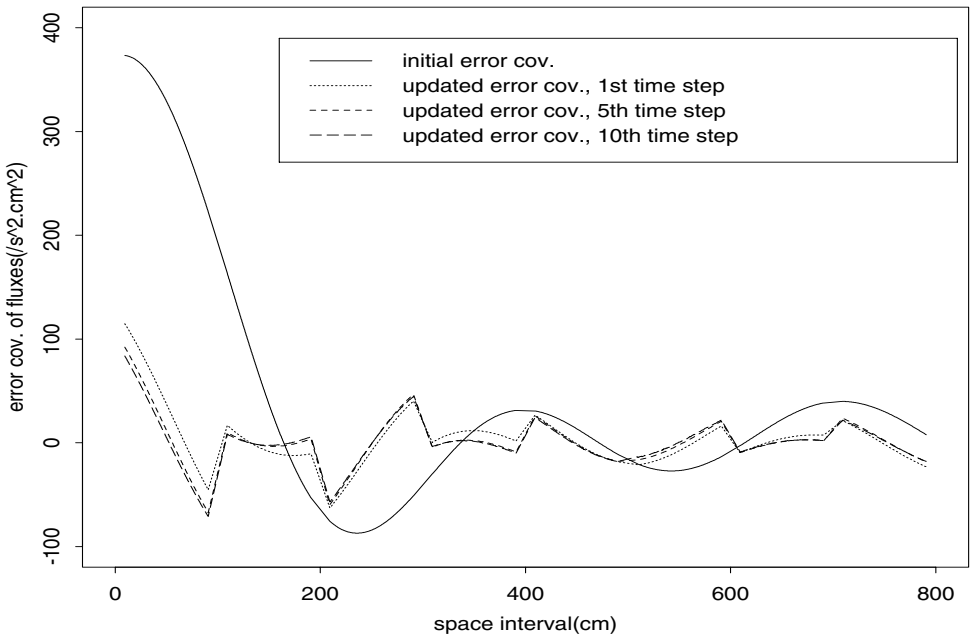

FIG. 5.8. *Updated error covariances of microscale fluxes at different time steps;* $N_e = 500$*; mesh size* $= 0.5cm$.

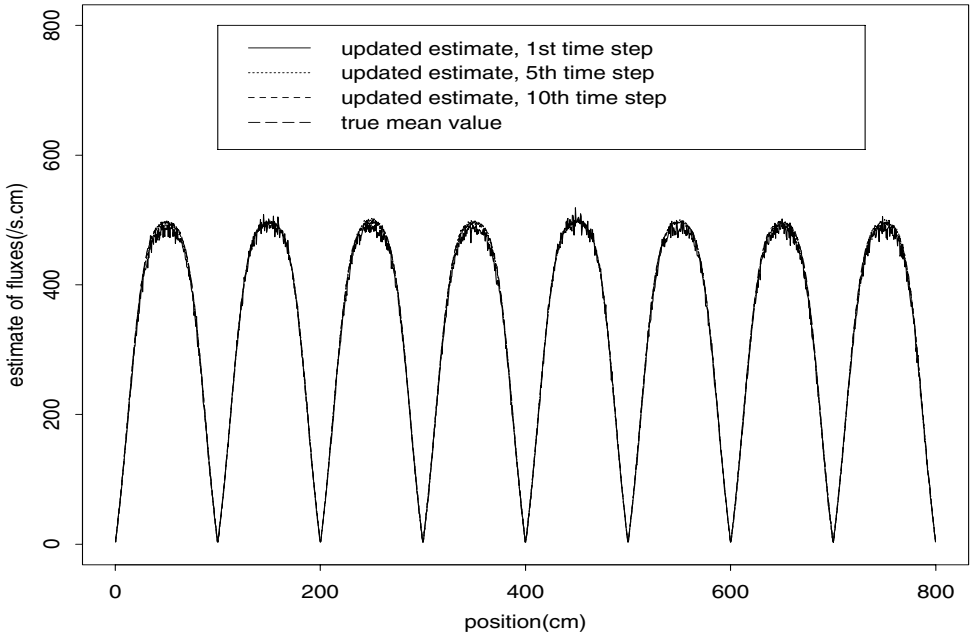

FIG. 5.9. *Updated estimates of macroscale fluxes at different time steps;* $N_e = 500$*; mesh size* $= 0.5cm$.

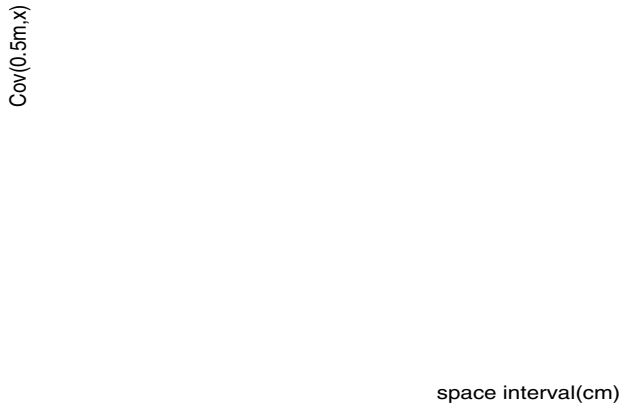
Cov(0.5m,x)
space interval(cm)

6. Conclusions and remarks. A multiscale data assimilation approach using the EnKF method is suggested in the present paper to estimate particle fluxes across different scales in boundaries with arbitrary profiles. To implement this approach, a multiscale bridging model is constructed to predict coarser-scale particle fluxes from finer-scale fluxes by considering particles with transverse Brownian motion. Instruments can be laid out at locations in different scales to provide observations for the estimation. An initial guess on the statistics of the microscale particle fluxes must be available a priori for the implementation of the proposed multiscale data assimilation approach. An example is used to verify the effect of this approach, and the results show that it can effectively estimate the statistical properties of flux processes. Although this example is dedicated to estimation of particle fluxes, the multiscale data assimilation method proposed in this paper can also be used to estimate the diffusion coefficient D and particle velocity V. The statistics of the macroscale particle fluxes can be used as boundary conditions for numerical simulations, such as LES, of particle transport problems such that efforts to take fine-scale fluxes as boundary conditions can be avoided.

REFERENCES

[1] G. Evensen, *Sequential data assimilation with a nonlinear quasi-geostrophic model using Monte Carlo methods to forecast error statistics*, J. Geophys. Res., 99 (1994), pp. 10143–10162.

[2] A. Gelb, *Applied Optimal Estimation*, The MIT Press, Cambridge, MA, 1974.

[3] R. N. Miller, M. Ghil, and F. Gauthiez, *Advanced data assimilation in strongly nonlinear dynamical systems*, J. Atmospheric Sci., 51 (1994), pp. 1037–1056.

[4] I. I. Gihman and A. V. Skorohod, *Stochastic Differential Equations*, Springer, New York, Heidelberg, 1972.

[5] F. D. Giovanni and P. M. Beckett, *On the mathematical modeling of pollen dispersal and deposition*, J. Appl. Meteorology, 29 (1990), pp. 1352–1357.

[6] A. Jazwinski, *Stochastic Processes and Filtering Theory*, Academic Press, New York, 1970.

[7] R. E. Kalman, *A new approach to linear filtering and prediction problems*, Trans. ASME J. Basic Eng., 82 (1960), pp. 35–45.

[8] R. E. Kalman and R. S. Bucy, *New results in linear filtering and prediction theory*, Trans. ASME J. Basic Eng., 83 (1961), pp. 95–108.

[9] J. Kevorkian, *Partial Differential Equations: Analytical Solution Techniques*, Springer, New York, 2000.

[10] P. J. Mason and S. H. Derbyshire, *Large eddy simulation of the stably stratified atmospheric boundary layer*, Boundary Layer Meteorology, 53 (1990), pp. 117–162.

[11] R. H. Reichle, D. B. Mclaughlin, and D. Entekhabi, *Hydrologic data assimilation with the ensemble Kalman filter*, Mon. Wea. Rev., 130 (2001), pp. 103–114.

[12] M. Germano, U. Piomelli, P. Moin, and W. H. Cabot, *A dynamic subgrid-scale eddy viscosity model*, Phys. Fluids A, 3 (1991), pp. 1760–1765.

[13] V. Armenio, U. Piomelli, and V. Fiorotto, *Effect of the subgrid scales on particle motion*, Phys. Fluids, 11 (1999), pp. 3030–3042.

[14] R. H. Shaw and U. Schumann, *Large-eddy simulation of turbulent flow above and within a forest*, Boundary Layer Meteorology, 61 (1992), pp. 47–64.

[15] M. Shinozuka, *Monte Carlo solution of structural dynamics*, Computers & Structures, 2 (1972), pp. 855–874.

[16] C. Soize, *The Fokker-Planck Equation for Stochastic Dynamical Systems and Its Explicit Steady State Solutions*, World Scientific, River Edge, NJ, 1994.

[17] G. Burgers, P. J. van Leeuwen, and G. Evensen, *Analysis scheme in the ensemble Kalman filter*, Mon. Wea. Rev., 126 (1998), pp. 1719–1724.

[18] Q. Z. Wang and K. D. Squires, *Large eddy simulation of particle-laden turbulent channel flow*, Phys. Fluids, 8 (1996), pp. 1207–1223.